CIVIL ENGINEERING JOURNAL

Article no. 29

THE CIVIL ENGINEERING JOURNAL 3-2024

# FRACTURE ENERGY OF UNSTABILIZED RAMMED EARTH: INFLUENCE OF CLAY TYPE AND CONTENT IN THE MIXTURE

*Barbora Mužíková, Tereza Plaček Otcovská and Pavel Padevět*

*Czech Technical University in Prague, Faculty of Civil Engineering, Department of Mechanics, Thákurova 7, 166 29 Praha 6, Czech Republic; barboramuzikova@seznam.cz*

## ABSTRACT

This study explores the fracture energy of unstabilized rammed earth, focusing on the influence of different types and amounts of clay within the mixtures. Utilizing a three-point bending test, this research evaluates the fracture energy of rammed earth to better understand how variations in clay type and content affect its structural integrity. The findings reveal significant differences in fracture energy values correlated with the clay's molecular structure and the interlayer chemical bonds. Clays such as illitic-kaolinitic, montmorillonite, and illite were tested, each demonstrating unique responses to mechanical stress based on their respective chemical bonds. Mixtures containing illitic-kaolinitic clay exhibited the highest fracture energy values, attributed to the presence of kaolinite due to its robust interlayer bonds. The results contribute insights into the selection and optimization of rammed earth materials for sustainable construction, aligning with the growing emphasis on ecological and durable building resources.

## KEYWORDS

Rammed earth, Clay, Fracture energy, Three-point bending test, Sustainable construction

## INTRODUCTION

The construction and materials engineering industry is grappling with the challenge of sourcing sustainable materials that also fulfill strict standards for durability and environmental impact. Unfired earth, traditionally perceived as an obsolete material, holds significant potential for modern applications. This article examines unstabilized rammed earth, a material with a rich historical legacy. As global focus on sustainability escalates, especially after 2023, the hottest year on record [1], this ancient construction technique is resurfacing as a promising solution due to its low energy production, recyclability, and positive influence on indoor climate.

Earthen construction has deep roots in human history. Ancient civilizations utilized locally available resources such as stone, earth, and plant materials to build shelters, resulting in the construction of earthen structures across all continents and climate zones. Some of the oldest preserved structures date back to the Neolithic period at sites like Catalhoyuk in Turkey and Mohenjo-Daro in India. In Egypt, large earthen blocks were used for structures with Nubian vaults (circa 3500 BCE). In Morocco, the 11th-century Ait Ben Haddou stands as a prominent example of rammed earth architecture [2].

The cradle of earthen construction also includes America. In South America, Peru is home to some of the largest and most significant unfired clay structures, including the pyramids of Túcume in the Lambayeque Valley. These pyramids, built around 1100 AD, comprise 26 structures spread over 200 hectares. Constructed from adobe bricks, these pyramids served as important cultural and religious centers for the civilizations. The construction technique involved mixing clay with water and organic materials, forming bricks, and allowing them to dry naturally in the sun [3]. Similarly, in the southwestern United States, the Ancestral Puebloans (formerly known as the Anasazi) built

impressive pueblos using similar techniques. An example is the Taos Pueblo in New Mexico, which has been continuously inhabited for over a thousand years [4].

In Europe, the earliest known building using earth is a Bronze Age half-timbered house with clay wall infill. The oldest earthen wall in northern Europe was found at the Heuneburg fortification in Germany, dating back to the 6th century BCE [5]. In the Czech Republic, earth construction gained traction in the 13th and 14th centuries as it became a primary building material. The popularity increased after devastating fires in the 16th and 17th centuries, which spurred the use of fire-resistant earth structures. This led to widespread use of earth buildings in both rural and urban architecture. Many traditional earth structures in Moravia remain intact, along with half-timbered houses in northwestern Bohemia, combining wooden frames and earth infill [6].

Modern rammed earth construction meets stringent housing standards and offers numerous benefits. Known for its excellent thermal mass, rammed earth helps regulate indoor temperatures, reducing the need for artificial heating and cooling, and is inherently fire-resistant. Studies by Bui [7] and Reddy [8] show that rammed earth walls exposed to natural weathering for 20 years have minimal erosion, demonstrating their long-lasting nature. These walls also provide good acoustic insulation, creating a quieter indoor environment, and their unique natural aesthetic blends well with various surroundings. Moisture absorption is a significant concern for rammed earth. Stabilizing agents like lime or cement are often added to reduce absorbency and improve moisture resistance. Stabilized rammed earth walls can effectively manage moisture levels, preventing mold growth and structural weakening [2]. Additionally, properly composed unfired clay can regulate indoor humidity between 40–60%, which is optimal for human health, and can bind harmful substances from the air (phthalates, formaldehyde, cigarette smoke) [9]. Stabilized rammed earth walls with hydraulic lime prevent moisture ingress, ensuring a healthier living environment [10].

For example, a family home in Santa Fe, New Mexico, features two substantial rammed earth walls (see Figure 1, left) [11]. In Plavy, Czech Republic, a traditional timber barn was reconstructed using stone and earth blocks, demonstrating the material's adaptability (see Figure 1, right) [12].

*Fig. 1 – Modern rammed earth buildings: on the left, a house in Santa Fe [11] and on the right, in Plavy [12]*

## Regulatory Challenges and Objectives

The adoption of earthen construction techniques in the EU is stymied by the absence of cohesive regulatory standards, partly due to its historical decline in the 19th century. During that period, the method of firing bricks in a circular kiln was discovered, dramatically reducing their cost. This regulatory gap relegated earthen construction mainly to enthusiasts and environmentally conscious individuals [13, 14]. Meanwhile, non-EU countries like Australia [15], New Zealand [16], and the USA (New Mexico) [17] have established specific regulations, though standards, particularly regarding mechanical properties, vary significantly. The required compressive strength ranges from 0.30 to 2.07 MPa, and tensile strength ranges from 0.00 to 0.35 MPa. In the EU, old standards for

earthen construction in Germany [18] and Switzerland [19] are no longer valid. This article seeks to bridge this knowledge gap by investigating how the composition of rammed earth - the type and quantity of clay, affects its fracture energy – one of crucial mechanical properties.

## MATERIALS AND METHODS

### Composition of the earth mixture

Earth forms through rock erosion due to mechanical movements like glaciers, wind, water, thermal expansion, and contraction, as well as chemical reactions with acids and oxygen. This results in clay, a mix of weathered rocks and organic components. The composition and properties of clay are influenced by local factors such as parent rock and climate. Thus, understanding the characteristics of a specific clay is crucial for construction use [2].

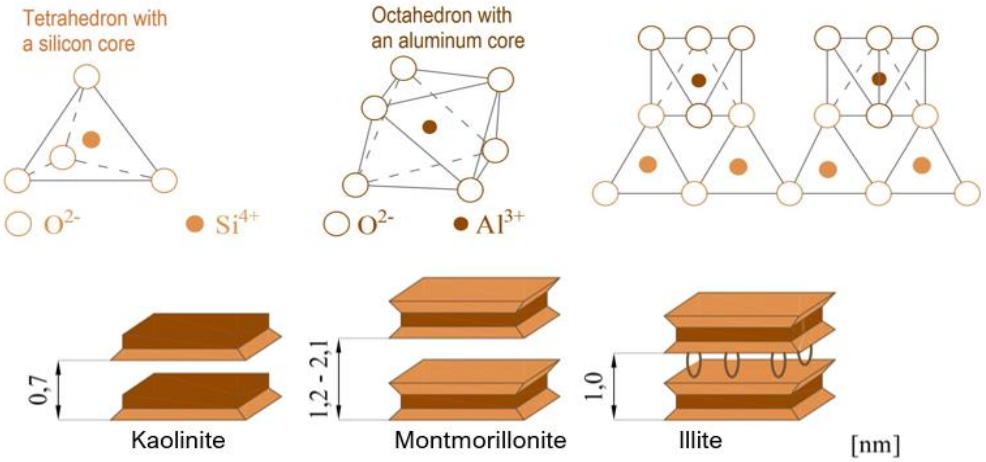


*Fig. 2 – Tetrahedron with a silicon core and octahedron with an aluminum core*

The earth is a mixture of fine particles like clay minerals, silt, sand, and other materials (gravel, stones, water). Silt, sand, and gravel are different from clay in that they are fillers bound by cohesive forces, consisting of eroded or water-transported aggregates. Their mutual ratio, known as granularity, is identified through sieve analysis, which determines the proportions and plots the grain-size curve [13]. In the mixture, clay acts as a binder, while larger particles act as fillers, and water activates clay's binding properties. The proportion and type of these components influence the earth's construction properties. "Clay is a natural material primarily composed of fine-grained minerals, generally plastic with adequate water content, and hardens upon drying or firing" [20]. Clay consists mainly of the phyllosilicate group, where large ions form layers, and smaller cations (Si, Al, Mg, Fe) occupy spaces between. These layers are structured as tetrahedra and octahedra (Figure 2). A structure composed of one tetrahedral and one octahedral layer is referred to as 1:1. The 2:1 layer type has two tetrahedral layers with one octahedral layer. Tetrahedral networks surround the octahedral one in the middle [20], see Figure 2.


*Fig. 3 – The pure clays used in the mixtures, images of the manufacturing test specimens, the process of ramming, and the manufactured specimens*

There are three main groups of clay minerals – kaolinite, smectite minerals, and illite. Kaolinite minerals, such as kaolinite, are hydrated aluminium silicates and are part of the 1:1 layered silicates. Adjacent layers of kaolinite are shifted by 0.7 nm and linked through hydrogen bonds and van der Waals forces, preventing swelling between layers and resulting in strong bonds. Smectite minerals, like montmorillonite, have a 2:1 layered structure and are characterized by weak van der Waals forces between layers, allowing water to penetrate between layers, causing swelling. Montmorillonite contains exchangeable cations that offset the negative charge of the layers. Illite, a 2:1 mineral, is structurally similar to montmorillonite but has stronger interlayer bonds and does not expand upon contact with water, although its bonds are not as strong as those in kaolinite [20].

Clay type is determined through methods like X-ray diffraction, which identifies clay minerals [2]. Next method is the methylene blue test, measuring dye absorption based on microstructure [21]. Atterberg limits define changes in clay properties with moisture, identifying transitions between liquid, plastic, and semi-solid states [22].

## Manufacturing of Specimens

The first step before manufacturing was to design the composition of the earth mixtures. The key objective during the development of the formulas was to investigate the effect of different types and amounts of clay, as well as adjusted water content, on the mechanical and physical properties of the manufactured specimens. Mixtures with different types of clay, various clay contents, and water contents were designed to enable comparison and to evaluate the impact of composition changes on the properties. The rammed earth was without stabilizers or other additives. The proposed sand-to-clay ratio was expressed as *s/c* in weight percentage of the mixture. The total sum of *s* and *c* was 100 %. The water coefficient *w* was then determined, representing the ratio of the water weight used in the mixture to the weight of the clay. The weight percentages of water in the mixture *h* were also determined for each mix, indicating the water content as a percentage of the total mixture weight.

*Tab. 1 - The chemical composition of clays used to produce test specimens. The percentage representation of individual compounds is given [29]*

| Type of clay | $SiO_2$ [%] | $Al_2O_3$ [%] | $Fe_2O_3$ [%] | $TiO_2$ [%] | CaO [%] | MgO [%] | $NA_2O$ [%] | $K_2O$ [%] |
|---|---|---|---|---|---|---|---|---|
| Illitic-kaolinitic (IK) | 59.31 | 24.71 | 3.37 | 1.09 | 0.19 | 0.40 | 0.30 | 2.82 |
| Illitic (I) | 56.57 | 18.40 | 9.72 | 1.16 | 1.12 | 2.54 | 0.18 | 2.91 |
| Montmorillonitic (M) | 50.51 | 31.20 | 3.37 | 0.86 | 0.40 | 0.42 | 0.08 | 1.62 |

Three types of clays were used (illitic-kaolinitic S and KR, illitic AGL, and montmorillonite GEM), all supplied in powder form (see Figure 3) by LB Minerals. The exact chemical composition of the clays used is in Table 1. (except clay S, which did not have the exact chemical composition listed). The clays were mixed with sand of known grain-size distribution in predefined ratios, and the grain-size curves of each mixture were then calculated, there are shown in Figure 4. Along with the grain-size curves of the mixtures used in this paper, some grain-size curves of rammed earth mixtures used in the literature are included in the Figure 4 for a better general idea. For producing the test specimens, the mixture components were weighed according to predetermined formulations. First, the exact amount of sand and water was weighed, then 2/3 of the water was added to the sand and mixed. Finally, the clay and the remaining water were added, and the entire mixture was thoroughly blended. Water for the mixture was sourced from the municipal water supply.

The mixtures were compacted into steel molds, using both mechanical and manual compaction methods to ensure material homogeneity. There were two basic specimen sizes: 40×40×60 mm and 20×20×100 mm. After being removed from the molds, the prepared specimens were transferred to a controlled drying process in a climate chamber to ensure a stable environment before measuring their properties. Nineteen mixtures were produced, and 3 to 6 specimens from each were tested in the three-point bending test.

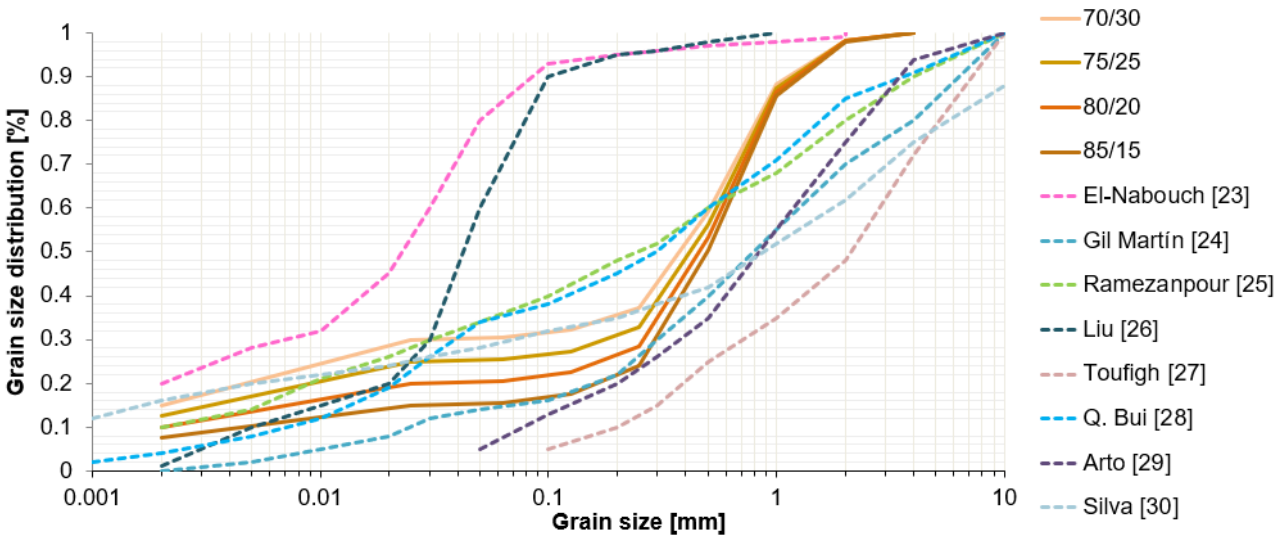


*Fig. 4 – Grain size distribution curves of the used mixtures, marked sand/clay ratio (solid lines) and comparison with grain size curves from the literature (dashed lines)*

Due to laboratory constraints, such as the limited force of the testing machine, smaller samples of rammed earth with reduced layer height compared to real-world structures were used in this study. The maximum grain size in the mixture was set to 4 mm. Based on this grain size, the number of compacted layers at a height of 40 mm was set to 4-5 (at least 8 mm each), and at a height of 20 mm to 3 layers (at least 6 mm each). The layer thickness was ensured to be at least 1.5 times greater than the maximum grain size to maintain structural integrity and layer representativeness. The mechanical properties of larger structures can be effectively replicated at a

smaller scale if layering principles are followed. The authors believe that these conditions still provide a valid approximation of the behaviour of rammed earth.

## Fracture Energy of Rammed Earth: State of the Art

Fracture mechanics examines the failure of materials beyond traditional strength analysis, focusing on the energetic analysis needed for crack formation. There are three main types of fracture mechanics: linear, which applies to brittle materials with inelastic deformation at the crack tip; elastic-plastic, for ductile materials like steel that develop a plastic, strengthening, nonlinear zone around the crack tip; and nonlinear fracture mechanics for quasi-brittle materials like concrete or unstabilized rammed earth, which develop a nonlinear process zone with gradual damage in the form of microcracks and microslips. This can be seen in Figure 4 [31, 32]. For clarification, mode I fracture, where the crack opens, is depicted in Figure 4.

Before conducting experimental measurements, a review of current studies on fracture energy in unstabilized rammed earth was performed. Table 2 lists fracture energy values from the literature, including the author's name, the country of research, and the publication reference. It provides bulk density $\rho$, flexural tensile strength $f_t$, and its standard deviation (if reported). Another column indicates the method used to determine fracture energy, followed by the fracture energy value $G_f$ and its standard deviation (if reported).

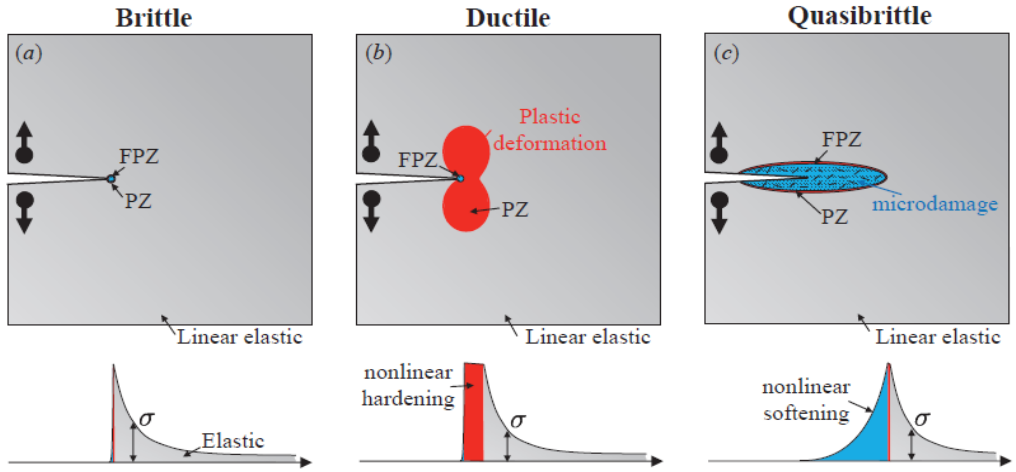


*Fig. 4 – Types of structural fracturing behaviour: (a) brittle, (b) ductile and (c) quasi-brittle. Trends of the stress distributions along the crack line are shown at the bottom of each figure [31]*

Since rammed earth is classified as a quasi-brittle material, fracture energy is a critical property alongside compressive and tensile strength and the modulus of elasticity. Despite its importance for understanding material behaviour and potential mathematical modelling, it has received relatively little research attention.

*Tab. 2 - Fracture energy values reported in the literature*

| Source | $\rho$ [kg/m$^3$] | $f_t$ [MPa] | Type of test | $G_f$ [J/m$^2$] |
|---|---|---|---|---|
| Q. Bui (VN) [28] | 2300 | 0.130 | Calculated of $f_c$, depends on grain size | 12 |
| Arto (ES) [29] | 2010 | 0.440 ± 0.050 | Three-point bending test | 23 |
| Silva (PT) [30] | 1830 | 0.126 | Estimated as 29$f_t$ | 4 |
| Miccoli (DE) [33] | 2190 | 0.370 | Estimated as 29$f_t$ | 11 |
| Corbin (GB) [34] | - | - | Wedge splitting test | 2 ± 1 |
| Hussaini (IR) [35] | 1946 | 0.240 | Wedge splitting test | 19 |

## Method for Measuring and Calculating Fracture Energy

The three-point bending method was chosen to measure the fracture energy. Literature identifies two types of tests for obtaining fracture energy: three-point bending tests and wedge splitting tests. However, a challenge arises with the three-point bending of rammed earth due to difficulties in notch creation on the specimens. The specimens tend to crumble and break during cutting, thereby degrading the sample. Consequently, a modification of the standard methodology recommended was implemented, and the tests were performed without notches. Given that the mixture under test is fine-grained, a crack was anticipated to form under the applied load at mid-span without notching. This occurrence was confirmed experimentally (visible cracks are shown in Figure 5).

Rammed earth is generally assumed to be an anisotropic material. Tests, therefore, are conducted perpendicular to the rammed layers, aligning with the actual loading conditions of structural elements. This orientation posed challenges in test feasibility because the top edge was uneven due to the compaction process. This irregularity created difficulties in achieving a flat surface necessary for the load cylinder of the test rig. This led to the consideration of testing the samples in a rotated orientation, parallel to the compaction layers. In this setup, the two opposite sides of the body are flat, thanks to the steel mold used for specimen preparation.

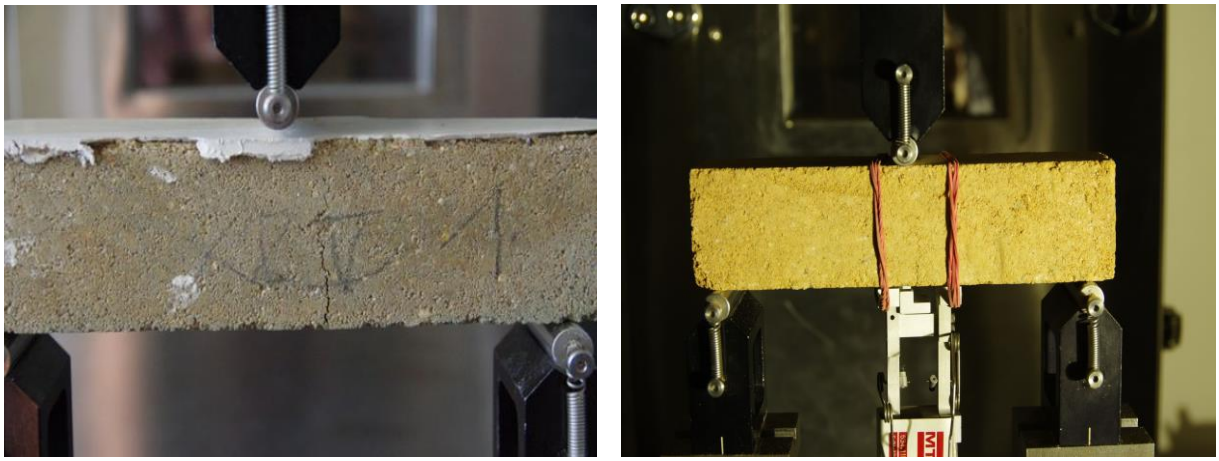

*Fig. 5 – Left: perpendicular [43], Right: parallel orientations of specimens*

Research on the anisotropy and isotropy of materials, such as the studies by T. Bui [36] and Q. Bui [37], were consulted. These studies, which investigated samples both perpendicular and parallel to the layers, demonstrated only a 5 % difference in compressive strength between these directions. Based on these findings, it was hypothesized that, assuming adequate adhesion between the layers, the material could be considered effectively isotropic for the purposes of this study, as reflected by the similar measured properties in both orientations. This assumption also supports the development of numerical models, such as those used by Silva [30] to model rammed earth as a homogeneous material.

Experimentally, this hypothesis was tested by analyzing samples from one mixture both perpendicular and parallel to the layers (see Figure 5 left for perpendicular and Figure 5 right for parallel). For perpendicular testing, the top edge of the specimens was smoothed with a thin layer of gypsum to create a flat surface, which did not affect the flexural strength. The differences in flexural tensile strength between the perpendicular and parallel orientations fell within the standard deviations of the measurements, aligning with the research findings where deviations were within 5 %. Additionally, no delamination occurred during the tests. Further bending tests were conducted on rotated specimens to avoid the need for plastering.

The fictitious crack model methodology was employed to determine fracture energy. This model addresses mode I (i.e., crack opening) where the crack is located on the axis of symmetry of the specimen and the load attempts to open the crack symmetrically [38]. For this determination, a

working diagram from a three-point bending test is essential. The tests were conducted using an MTS Alliance RT 30kN machine with a loading rate of 0.5 mm/min. The entire working diagram, including the descending branch, was recorded to capture the complete behaviour until specimen failure [38].

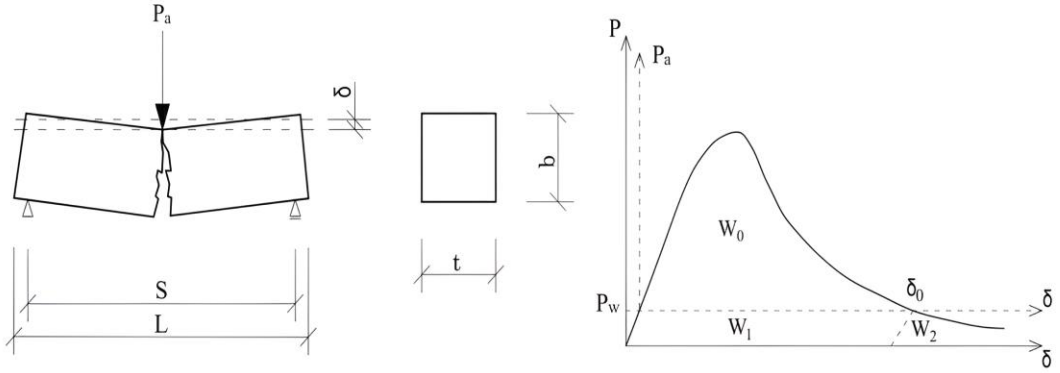


*Fig. 6 – Left: three-point bending arrangement, Right: obtained P-δ diagram*

The area that appears under the diagram is called the fracture work and from this the fracture energy $G_f$ can be calculated. Figure 6 shows a schematic of the test and the resulting working diagram with the added consideration of the self-weight. The area $W_0$ is the work done in three-point bending by the external loading force $P_a$. The force $P_w$ represents the equivalent force to the self-weight of the specimen. The areas $W_1$ and $W_2$ are due to the self-weight of the specimen. The area $W_1$ can be derived as $W_1 = P_w \cdot \delta_0$ [36]. The areas of $W_1$ and $W_2$ are equal according to [38].

Before calculating the fracture energy, the necessity of considering the stresses imposed on the crack by the specimen's own weight was evaluated. The stress over the midspan from the dead weight was compared to the tensile strength of the specimen, expressed as a percentage. This value, assessed across three different mixes, varied between 1.04–2.20 %. In the literature, it is recommended to include the self-weight in the fracture energy calculations for concrete, typically around 10 % [32]. Given the significantly lower values, the effect of self-weight was excluded from the fracture energy calculations in this study. The fracture work was then calculated using the area under the working diagram:

$$A_F = \int_0^{\delta_{max}} P(\delta) d\delta \quad (1)$$

Fracture energy was calculated by dividing the fracture work by the area of the crack created, expressed in units of N/m, or more specifically for this study, N/mm:

$$G_f = \frac{A_F}{b \cdot t} \quad (2)$$

## RESULTS

Fracture energy values are presented in Table 3. Each mixture is identified by a label provided by the clay manufacturer. Table columns include mixture number, number of specimens measured, specimen size, sand-to-clay ratio (*s/c*), water coefficient (*w*), clay content by weight percentage of the mixture (j), water content by weight percentage of the mixture (*h*), bulk density ($\rho$), bending tensile strength ($f_t$), fracture energy ($G_f$), and the standard deviation of the fracture energy ($\sigma_{Gf}$).

*Tab. 3 - Fracture energy measurement results*

| Mix. | No | Pcs | Size [mm] | *s / c – w* [% / % – - ] | Clay *j* [%] | Water *h* [%] | ρ *[kg/m3]* | $f_t$ [MPa] | $G_f$ [J/m$^2$] | $\sigma_{Gf}$ [J/m$^2$] |
|---|---|---|---|---|---|---|---|---|---|---|
| S | 3 | 6 | 20×20×100 | 75/25 – 0.295 | 23.3 | 6.9 | 2185 | 0.812 | 19.112 | 0.023 |
| S | 4 | 6 | 20×20×100 | 85/15 – 0.370 | 14.2 | 5.3 | 2064 | 0.373 | 7.438 | 0.037 |
| S | 5 | 6 | 20×20×100 | 75/25 – 0.335 | 23.1 | 7.7 | 2133 | 0.623 | 15.705 | 0.008 |
| GEM | 1 | 6 | 20×20×100 | 80/20 – 0.370 | 18.6 | 6.9 | 2097 | 0.344 | 17.335 | 1.460 |
| GEM | 2 | 6 | 20×20×100 | 75/25 – 0.370 | 22.9 | 8.5 | 2078 | 0.401 | 17.111 | 3.415 |
| GEM | 3 | 4 | 20×20×70 | 75/25 – 0.295 | 23.3 | 6.9 | 1932 | 0.361 | 16.577 | 1.804 |
| AGL | 1 | 3 | 40×40×160 | 80/20 – 0.370 | 18.6 | 6.9 | 2122 | 0.334 | 5.712 | 1.073 |
| AGL | 2 | 3 | 40×40×160 | 75/25 – 0.295 | 22.9 | 8.5 | 2082 | 0.330 | 8.389 | 1.141 |
| AGL | 3 | 3 | 40×40×160 | 80/20 – 0.400 | 18.5 | 7.4 | 2096 | 0.310 | 4.261 | 0.434 |
| AGL | 5 | 3 | 40×40×160 | 85/15 – 0.370 | 14.2 | 5.3 | 1982 | 0.146 | 1.933 | 0.308 |
| AGL | 6 | 3 | 40×40×160 | 85/15 – 0.400 | 14.2 | 5.7 | 1998 | 0.224 | 3.062 | 0.818 |
| AGL | 7 | 3 | 40×40×160 | 80/20 –0.290 | 18.9 | 5.5 | 2098 | 0.133 | 3.571 | 1.410 |
| AGL | 10 | 3 | 40×40×160 | 75/25 – 0.295 | 23.3 | 6.9 | 2125 | 0.328 | 7.410 | 0.634 |
| AGL | 11 | 3 | 40×40×160 | 75/25 –0.400 | 22.7 | 9.1 | 2095 | 0.386 | 9.776 | 0.787 |
| AGL | 12 | 3 | 40×40×160 | 70/30 –0.295 | 27.6 | 8.1 | 2097 | 0.458 | 10.997 | 1.475 |
| KR | 2 | 3 | 40×40×160 | 75/25 – 0.370 | 22.9 | 8.5 | 2098 | 0.695 | 21.944 | 4.702 |
| KR | 8 | 3 | 40×40×160 | 80/20 –0.290 | 18.9 | 5.5 | 2052 | 0.551 | 11.613 | 2.302 |
| KR | 11 | 3 | 40×40×160 | 75/25 – 0.400 | 22.7 | 9.1 | 2115 | 0.638 | 20.746 | 6.057 |
| KR | 14 | 3 | 40×40×160 | 70/30 – 0.400 | 26.8 | 10.7 | 2112 | 0.678 | 14.069 | 1.256 |

Mixture KR 2 exhibited the highest fracture energy, measuring 21.944 ± 4.702 J/m², whereas the lowest was observed in AGL 3 at 1.933 ± 0.308 J/m². These results, discussed in further detail in the subsequent chapter, correspond well with the mixture's composition. The observed values align with the range reported in the literature, as referenced in Table 2. For instance, the minimum value closely matches the 2 J/m² reported by Corbin [39] and the 4 J/m² by Silva [30], adjusted to equivalent units. The maximum value of 23 J/m² from Arto work [34] aligns with our highest measurements. Average values noted by Q. Bui [28] at 12 J/m² and Miccoli [33] at 11 J/m² correspond to our mean measurements, underscoring the consistency of our data with existing studies. The graph in Figure 7 compares the measured fracture energies of the different mixtures. Each clay is indicated by a different colour of the bars. The orange markers plot the percentage of clay in the mixture and the blue markers plot the water content. For a detailed analysis of the impact of composition, the mixtures were divided into two groups. These groups were defined so that each group shared a common characteristic in the composition:

*Type of Clay:* Mixtures in this group have identical composition except for the type of clay used. The sand-to-clay ratio (s/c) and the water coefficient *w* are the same.

*Different Clay Content:* Mixtures here have the same water coefficient w, but the clay content varies among the mixtures. However, all mixtures in this group utilize the same type of clay.

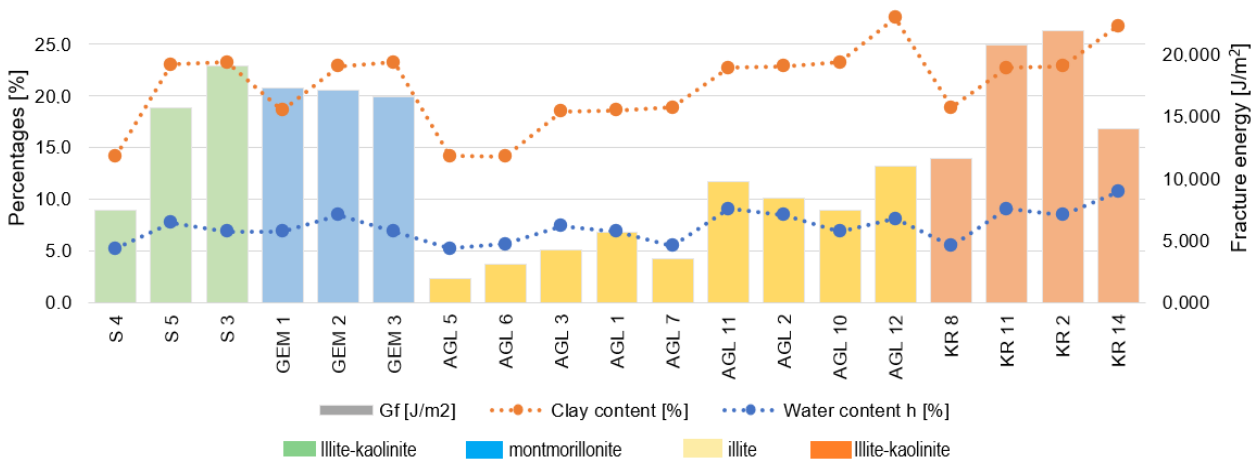


*Fig. 7 – Results of fracture energies with indicated percentages of clay and water in the mixture*

## Type of Clay

The first comparative set includes mixtures with the same sand-to-clay ratio (s/c) and water coefficient but different types of clay. For the KR mixture, the clay is illitic-kaolinitic (IK, S), while the AGL group contains illitic clay (I), montmorillonite (M).

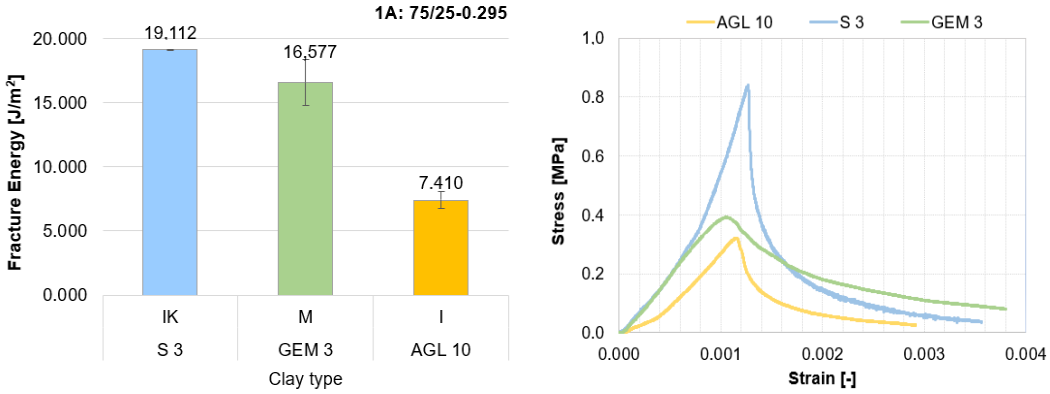


*Fig. 8 – Left: Fracture energy for group 1A, Right: Stress-Strain diagrams of 1A*

*1A: 75/25–0.370:* The highest fracture energy was measured in the S3 mixture containing illitic-kaolinitic clay, reaching 19.112 ± 0.023 J/m$^2$. The mixture with montmorillonite clay, GEM 3, followed with 16.577 ± 1.804 J/m$^2$. The lowest value was observed in the AGL10 mixture with illite, recording 7.410 ± 0.634 J/m$^2$. The results are graphically compared in Figure 8.

*1B: 75/25–0.400:* Mixtures in this group have a higher water coefficient than group 1A with the same sand/clay ratio. Again, the highest value was observed in the KR 2 mixture with illitic-kaolinitic clay, amounting to 21.944 ± 4.702 J/m$^2$. The mixture with montmorillonite, GEM 2, showed slightly lower values at 17.111 ± 3.415 J/m$^2$, and the smallest value was recorded in the AGL 2 mixture with illite, showing 8.389 ± 1.141 J/m$^2$. The values are displayed graphically in Figure 9.

*1C: 80/20–0.290:* In this group, the highest fracture energy value was measured in the GEM 1 mixture with montmorillonite, which was 17.355 ± 1.460 J/m$^2$. The smallest value was recorded in the AGL 1 mixture with illitic-kaolinitic clay, measuring 5.712 ± 1.073 J/m$^2$.

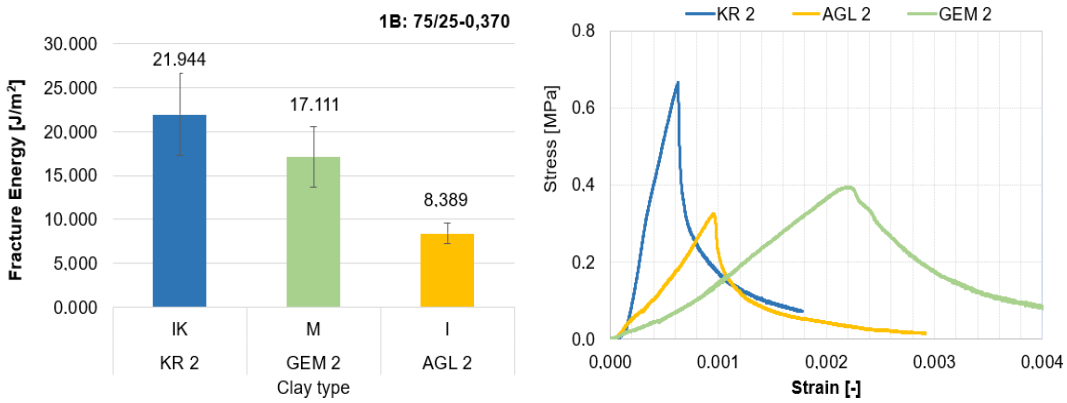


*Fig. 9 – Left: Fracture energy for group 1B, Right: Stress-Strain diagrams of 1B*

*1D: 85/15–0.370:* Higher values were measured in the S 4 mixture with IK clay, 7.4385 ± 0.037 J/m$^2$, while the smaller value was observed in the AGL 5 mixture with I clay, at 1.933 ± 0.308 J/m$^2$.

Across all comparative groups, the highest values were observed in mixtures with illitic-kaolinitic clay, followed by montmorillonite clay, with the lowest values consistently recorded in mixtures with illitic clay.

## Different Clay Content

In Group 2, mixtures with the same water coefficient, same type of clay but differing in the clay content are compared.

*2A: w=0.295, Illite Clay:* There are two mixtures, AGL 10 with 23.3 % clay and AGL 12 with 27.6 % clay. The higher fracture energy value was observed in mixture AGL 12 with a higher clay content (10.997 ± 1.475 J/m²), while a lower value was measured for mixture AGL 10 with less clay (7.410 ± 0.634 J/m²).

*2B: w=0.370, Illite Clay:* A similar trend is found in group 7B again with illite, but with a higher water coefficient w=0.370. The lowest value is in mixture AGL 5 with 14.2 % clay (1.933 ± 0.308 J/m²), followed by mixture AGL 1 with 18.6 % clay (5.712 ± 1.073 J/m²), and the highest value was measured in mixture AGL 2 with 22.9 % clay (8.389 ± 1.141 J/m²), see Figure 10.

*2C: w=0.400, Illite Clay:* Group 7C is the last with illite and the highest water coefficient w=0.400. Graphical comparison of the measured values is shown in Figure 11. Again, a trend is observed where the fracture energy increases with the clay content. The lowest fracture energy value of 3.062 ± 0.818 J/m² was measured for AGL 6 with 14.2 % clay, followed by mixture AGL 3 with 4.261 ± 0.434 J/m² and 18.5 % clay, and the highest value of 9.776 ± 0.787 J/m² was for mixture AGL 11 with the highest clay content of 22.7 %.

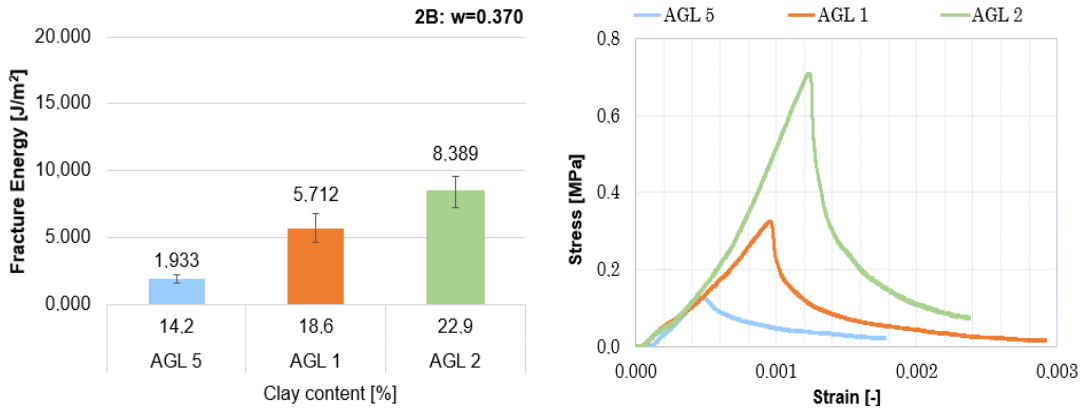


*Fig. 10 – Left: Fracture energy for group 2B, Right: Stress-Strain diagrams of 2B*

*2D: w=0.400, Illitic-Kaolinitic Clay:* Unlike the previous groups with illite, the highest fracture energy value of 20.746 ± 6.057 J/m² was measured for mixture KR 11 with a lower clay content of 22.7%, while a lower value of 14.069 ± 1.256 J/m² was measured for mixture KR 14 with a higher clay content of 26.8 %.

*2E: w=0.400, Montmorillonite Clay:* The last group consists of mixtures with montmorillonite. Two mixtures, GEM 1 with 18.6 % clay and GEM 2 with 22.9 % clay, had comparable fracture energy values of 17.355 ± 1.460 J/m² and 17.111 ± 3.415 J/m², respectively.

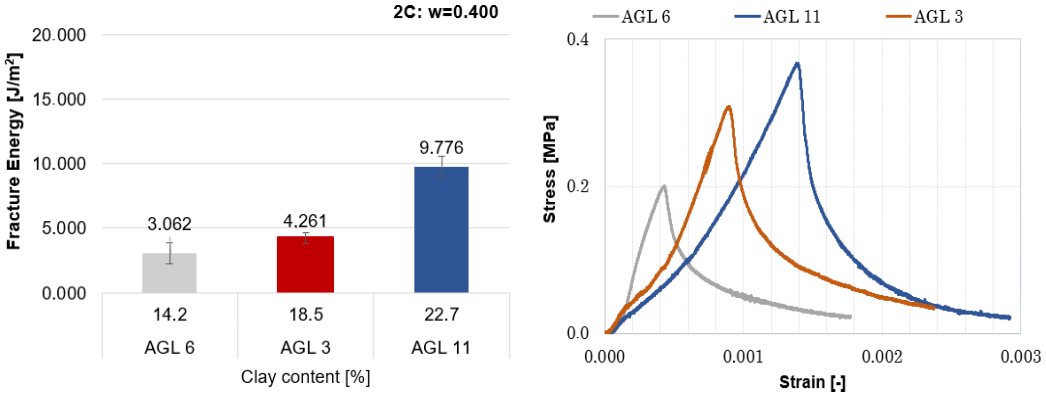


*Fig. 11 – Left: Fracture energy for group 2C, Right: Stress-Strain diagrams of 2C*

Across all tested groups with illite, an increasing trend in fracture energy was noted with the rising clay content. However, the results for illitic-kaolinitic clay deviated from the expected trend; surprisingly, mixtures with a lower content of this clay type showed higher fracture energy, suggesting an influence of kaolinite's properties enhancing the material's performance even at lower concentrations. This unexpected outcome highlights the complex interplay of clay composition on mechanical properties. For montmorillonite mixtures, the fracture energy values were relatively uniform, indicating that the impact of varying clay content is less pronounced due to the clay's inherent susceptibility to water-induced swelling, aligning with its known properties.

## Fracture Energy and Tensile Strength in Bending Relationship

From the measured data on fracture energy and tensile strength in bending, a correlation coefficient of R = 0.77 was established, indicating a strong correlation. The relationship derived from the data is as follows: $G_f = 24f_t$. However, this relationship may not be universally applicable, as it is only a calculation based on the measured data, serving as a rough estimate of the dependence of fracture energy on flexural tensile strength. Interestingly, the work by Silva [30] and Miccoli [33], who did not measure fracture energy experimentally but inferred it from tensile strength, used the relationship $G_f = 29f_t$, which is close to the results obtained from the experiments presented in this article.

## DISCUSSION

Mixtures containing illitic-kaolinitic clay demonstrated the highest fracture energy values, influenced by the strong interlayer bonds of kaolinite. These strong bonds, formed via hydrogen bonds and van der Waals forces, prevent moisture-induced swelling and enhance the mechanical stability of the material [2]. In contrast, montmorillonite mixtures exhibited lower fracture energy due to their naturally weaker van der Waals bonds. These bonds facilitate water penetration and swelling, compromising structural integrity under load [20]. Although montmorillonite contains exchangeable cations that provide cohesion and resistance, they do not sufficiently counteract the mechanical weakening associated with its structural properties. While illite has stronger interlayer bonds than montmorillonite [20], it showed the lowest fracture energy values among the tested clays. This suggests that although illite bonds resist water-induced expansion better than montmorillonite, they

are significantly weaker than kaolinite bonds, limiting their effectiveness in enhancing the fracture energy of rammed earth.

When comparing clay content in the mixtures, an increasing trend in fracture energy was observed for illite across all test groups with rising clay content. However, results for illitic-kaolinitic clay deviated from this expected trend. Mixtures with a lower content of this clay demonstrated higher fracture energy, indicating kaolinite properties that improve material performance even at lower concentrations. This unexpected result emphasizes the complex interplay between clay composition and mechanical properties. In montmorillonite mixtures, fracture energy values were relatively consistent, suggesting that varying clay content has a less pronounced impact. These measurement results indicate the significant impact of both the type and content of clay on the fracture energy of rammed earth. While previous studies typically focused on individual clay types, such as Corbin [36] with kaolinite, or mixtures of multiple types of clay (Miccoli [33], el Nabouch [23]), other articles do not specify the exact type and chemical composition of clay. Instead, they measure only the clay content based on the particle size distribution curve (e.g., Silva [30], Arto [29]). This article examines three specific types of clay and shows that the clay type significantly influences the mechanical properties of rammed earth.

## CONCLUSION

This study confirms the critical impact of the type and amount of clay on the fracture energy of unstabilized rammed earth. It was found that mixtures containing illitic-kaolinitic clay exhibit the highest fracture energy values, attributed to the presence of kaolinite. The robust interlayer bonds of kaolinite enhance the structural integrity and resilience of the earth. Montmorillonite, with its weaker bond structure, showed lower fracture energy values. Illite, despite having stronger bonds than montmorillonite but weaker than those of kaolinite, still displayed the lowest fracture energy.

Unexpectedly, the study revealed that even the low mechanical properties of earth can be optimized by adjusting the content and type of clay in the mixture. This finding differs from traditional approaches that do not differentiate between the types of clays contained in the mixture. Given these insights, further research should focus on exploring the detailed mechanical behaviours of different types of clays under various environmental conditions and stresses, to develop more accurate predictions and models for the behaviour of rammed earth.

## ACKNOWLEDGEMENTS

This research was supported by project SGS22/089/OHK1/2T/11 Building Materials and Construction through the Eyes of Experiment and from the project GACR No. 18-10884S Unfired and Rammed Clay for Construction.

## REFERENCES

[1] Copernicus, 2024. Global Climate Highlights 2023: Copernicus - 2023 is the hottest year on record, with global temperatures close to the 1.5°C limit. https://climate.copernicus.eu/copernicus-2023-hottest-year-record [cited 2024-09-01]

[2] Reddy, B.V.V., 2022. Compressed Earth Block & Rammed Earth Structures (Springer Nature Singapore, Singapore) Springer Transactions in Civil and Environmental Engineering. 331-345 pp. ISBN: 9789811678776.

[3] Taos Pueblo, 2024. About. https://taospueblo.com/about/ [cited 2024-07-16].

[4] Peru Hop, 2024. Tucume: Valley of the Pyramids, Peru. https://www.peruhop.com/tucume-valley-of-pyramids-peru/ [cited 2024-07-16].

[5] Minke, G., 2006. Building with Earth: Design and Technology of a Sustainable Architecture (Birkhäuser - Publisher for Architecture). 11-18 pp. ISBN: 9783764374778.

[6] Žabičková, I., 2002. Earthen Buildings (ERA Publishing). 1-15 pp. ISBN: 8086517217.

[7] Bui, Q. B., Morel, J.-C., Reddy, B., Ghayad, W., 2009. Durability of rammed earth walls exposed for 20 years to natural weathering. Building and Environment, vol. 44, 912-919 pp. DOI: 10.1016/j.buildenv.2008.07.001.
[8] Reddy, V. B. V., Kumar, P. P., 2011. Cement stabilized rammed earth Part B: Compressive strength and stress-strain characteristics. Materials and Structures, vol. 44, 695-707 pp. DOI: 10.1617/s11527-010-9644-7.
[9] Růžička, J., Diviš, J., 2019. The Influence of Building Materials on Relative Humidity of Internal Microclimate. IOP Conference Series: Earth and Environmental Science, vol. 290, 012029 pp. DOI: 10.1088/1755-1315/290/1/012029
[10] Hall, M., & Djerbib, Y., 2004. Rammed earth sample production: context, recommendations and consistency. Construction and Building Materials, vol. 18, no. 4, 281-286 pp. DOI: 10.1016/j.conbuildmat.2004.02.006.
[11] Nk'Mip Desert Cultural Centre, 2023. Southeast Wyoming Welcome Center. https://sirewall.com/portfolio/nkmip-desert-cultural-centre/ [cited 2023-05-15]
[12] Mutl, J., 2023. Implementation - Family House in Plavy. http://janmutl.cz/realizace/ [cited 2023-05-16]
[13] Houben, H., Guillaud, H., 1994. Earth Construction: A Comprehensive Guide (ITDG Publishing). 145-158 pp. ISBN: 1-85339-193-X.
[14] Keable, J., Keable, R., 1996. Rammed Earth Structures (Practical Action Publishing). 16-28 pp. ISBN: 978-1-85339-727-1.
[15] Walker, P., Standards Australia, 2002. HB 195 - 2002: The Australian Earth Building Handbook (Standards Australia). 40-45 pp. ISBN: 0-7337-4000-6.
[16] Council New Zealand, 1998. NZ 4297: Engineering design of earth buildings. http://www.eastue.org/project/linea-adobe/norme/NZD4297-1998-Engineering_Design_of_Earth_Buildings.pdf [cited 2023-05-22]
[17] Construction Industries Division of the Regulation and Licensing Department, 2016. 2015 New Mexico Earthen Building Materials Code. https://www.srca.nm.gov/parts/title14/14.007.0004.html [cited 2023-05-22]
[18] Deutscher Normenausschuss Fachnormenausschuss Bauwesen, 1956. Lehmbau: Ausführung von Lehmbauten: Richtlinien: DIN 18954 (Beuth).
[19] Schweizerischer Ingenieur- und Architekten-Verein, 1994. D 0111: Regeln zum Bauen mit Lehm. https://www.iglehm.ch/application/files/2515/1696/9453/SIA_D0111_Lehmbauregeln.pdf (cited 30-3-2024)
[20] Weiss, Z., Kužvart, M., 2005. Clay Minerals and Their Nanostructure and Uses (Karolinum, Prague). ISBN: 80-246-0868-5.
[21] Otcovská, T., Mužíková, B., Padevět, P., 2022. Methylene blue test and adsorption capacity of clays. Acta Polytechnica CTU Proceedings, vol. 34, 63 pp. DOI: 10.14311/APP.2022.34.0063
[22] Mitchell, J.K., Soga, K., 2005. Fundamentals of Soil Behavior (John Wiley & Sons, Inc.). 15-16 pp. ISBN: 978-0-471-46302-7.
[23] El-Nabouch, R., Bui, Q.-B., Plé, O., Perrotin, P., 2017. Assessing the in-plane seismic performance of rammed earth walls by using horizontal loading tests. Engineering Structures, vol. 145, pp. 153-161. DOI: 10.1016/j.engstruct.2017.05.027.
[24] Gil-Martín, L.M., Fernández-Ruiz, M.A., Hernández-Montes, E., 2022. Mechanical characterization and elastic stiffness degradation of unstabilized rammed earth. Journal of Building Engineering, vol. 56. DOI: 10.1016/j.jobe.2022.104805
[25] Ramezanpour, M., Eslami, A., Ronagh, H., 2021. Seismic performance of stabilised/unstabilised rammed earth walls. Engineering Structures, vol. 245. DOI: 10.1016/j.engstruct.2021.112982
[26] Liu, Q., Tong, L., 2017. Engineering properties of unstabilized rammed earth with different clay contents. Journal of Wuhan University of Technology-Mater. Sci. Ed., vol. 32, 914-920 pp. DOI: 10.1007/s11595-017-1690-y
[27] Toufigh, V., Kianfar, E., 2019. The effects of stabilizers on the thermal and the mechanical properties of rammed earth at various humidities and their environmental impacts. Construction and Building Materials, vol. 200, 616-629 pp. DOI: 10.1016/j.conbuildmat.2018.12.050
[28] Bui, Q.B., Bui, T.T., Tran, M.P., Bui, T.L., 2019. Assessing the Seismic Behavior of Rammed Earth Walls with an L-Form Cross-Section. Sustainability, vol. 11, issue 5. DOI: 10.3390/su11051450

[29] Arto, I., Gallego, R., Cifuentes, H., Puertas, E., Gutiérrez-Carrillo, M.L., 2021. Fracture Behavior of Rammed Earth in Historic Buildings. Construction and Building Materials, vol. 289. DOI: 10.1016/j.conbuildmat.2021.123196

[30] Silva, R., Oliveira, D., Schueremans, L., Lourenco, P., Miranda, T., 2014. Modelling of the Structural Behaviour of Rammed Earth Components. Proceedings of the 9th International Conference on Civil, Structural and Environmental Engineering Computing. DOI: 10.4203/ccp.106.112

[31] Bažant, Z., Le, J.L., Salviato, M., 2021. Quasibrittle Fracture Mechanics and Size Effect: A First Course (Oxford University Press, Oxford). 3-6 pp. ISBN: 978-0-19-284624-2.

[32] Shah, S., Carpinteri, A., 1991. Fracture Mechanics Test Methods For Concrete (Taylor and Francis, London). 162-165 pp. ISBN: 0-412-41100-8.

[33] Miccoli, L., Oliveira, D., Silva, R., Mueller, U., Schueremans, L., 2014. Static Behaviour of Rammed Earth: Experimental Testing and Finite Element Modelling. Materials and Structures, vol. 48. DOI: 10.1617/s11527-014-0411-7

[34] Corbin, A., Augarde, C., 2014. Fracture Energy of Stabilised Rammed Earth. Procedia Materials Science, vol. 3. DOI: 10.1016/j.mspro.2014.06.217

[35] Hussaini, S.M.S., Toufigh, V., 2019. Strength and Fracture Behavior of Rammed-Earth Materials. Journal of Materials in Civil Engineering, vol. 31, issue 10. DOI: 10.1061/(ASCE)MT.1943-5533.0002923

[36] Bui, T.T., Bui, Q.B., Limam, A., Maximilien, S., 2014. Failure of rammed earth walls: From observations to quantifications. Construction and Building Materials, vol. 51, 295-302 pp. DOI: 10.1016/j.conbuildmat.2013.10.053

[37] Bui, Q.B., Morel, J.C., 2009. Assessing the anisotropy of rammed earth. Construction and Building Materials, vol. 23(9), 3005-3011 pp. DOI: 10.1016/j.conbuildmat.2009.04.011

[38] Vydra, V., 2005. Habilitation thesis: Fracture characteristics of concrete exposed to high temperatures (Czech Technical University in Prague).